

Poiseuille flow of soft polycrystals in 2D rough channels

Tanmoy Sarkar,¹ Pinaki Chaudhuri,² and Anirban Sain^{1,*}

¹*Department of Physics, Indian Institute of Technology, Bombay, Powai, Mumbai-400 076, India.*

²*Institute of Mathematical Sciences, CIT Campus, Taramani, Chennai 600113, India*

(Dated: April 2, 2020)

Polycrystals are partially ordered solids where crystalline order extends over mesoscopic length scales, namely, the grain size. We study the Poiseuille flow of such materials in a rough channel. In general, similar to yield stress fluids, three distinct dynamical states, namely, flowing, stick-slip and jammed can be observed, with a yield threshold dependent on channel width. Importantly, the interplay between the finite channel width, and the intrinsic ordering scale (the grain size) leads to new type of spatiotemporal heterogeneity. In wide channels, although the average flow profile remains plug like, at the underlying granular level, there is vigorous grain remodelling activity resulting from the velocity heterogeneity among the grains. As the channel width approaches typical grain size, the flowing polycrystalline state breaks up into a spatially heterogeneous mixture of flowing liquid like patches and chunks of nearly static grains. Despite these static grains, the average velocity still shows a parabolic profile, dominated by the moving liquid like patches. However, the solid-liquid front moves at nearly constant speed in the opposite direction of the external drive.

I. INTRODUCTION

Dense colloidal emulsions are good model systems for studying polycrystalline and amorphous solids. Polycrystals have mesoscopically large ordered regions, the grains, which are separated by atomistically narrow disordered grain boundaries, across which the grain orientation changes abruptly [1]. In contrast, there is no spatial order in atomic arrangements, for amorphous materials. So, in terms of the degree of spatial heterogeneity, polycrystals fall in between single crystal and amorphous material [2]. How does the intrinsic ordering scale, the grain size, make polycrystals different in terms of dynamic response? It has been shown that sheared polycrystals, share some of the flow properties (vortices, saddles etc.) of amorphous material [1, 3], yet retaining unique features like grain rotation, dislocation creep etc. Experimental studies involving rheology of soft polycrystals have started to probe these questions [4–7].

Driven flow of such materials through a rough channel (e.g., under gravity or pressure gradient) requires that the applied force overcome the resistive friction from the channel walls. But the wall friction, due to no slip boundary condition, gives rise to velocity gradients and thereby can create a spatially non-uniform stress field. Can the polycrystal sustain these stress gradients or does it break down into a flowing amorphous state, when it yields? In this Letter, we probe this question.

In this letter, using molecular dynamics (MD) simulations, we report the flow response of a 2D soft polycrystalline system, confined in a rough channel and subjected to a constant body force (e.g., gravity), resulting in a Poiseuille flow. We demonstrate that the onset of steady flow depends on a yield threshold which decreases as the channel width is increased. Surprisingly, for wide channels, i.e., when $w \gg d$, the particle diameter, despite maintaining a polycrystalline morphology, a plug-like flow emerges, while grains continuously undergo break-up and coalescence within the plug. On the other hand, for narrow channels, when $w \approx 10d$, there is significant melting of the polycrystalline structure and interestingly, the fluid-solid front moves at a constant speed in the opposite direction of the main flow.

II. MODEL

For our study, we considered a weakly bi-disperse, two-dimensional Lennard-Jones (LJ) system with total number of particles $N = 12118$. By choosing the fraction of large particle as 1% and the size ratio of 1.4, we generate polycrystalline states [8]. We worked at volume fraction $\phi = 1$ and temperature $T = 0.2$. The weakly bi-disperse system can sustain a polycrystalline non-equilibrium steady state, under shear [9, 10], unlike the monodisperse system which tends to form single crystal when sheared. The 2D Poiseuille flow is set up in a rectangular box ($L \times w$) with two confining walls perpendicular to the y-axis and periodic boundary conditions along x axis. We apply driving force to an initial state which is a preformed polycrystalline sample prepared using the above parameters. To generate

* asain@phy.iitb.ac.in

the Poiseuille flow, only the particles within a slab, of width w , parallel to \hat{x} axis, centred around the middle of the box, were subjected to an additional constant external force $F_{ext}\hat{x}$. The static particles above and below the slab, which interact via the LJ potential with the flowing particles, serve as the rough channel walls. The width w of the slab was systematically varied to study the flow for different confinements. The temperature is maintained via a local thermostat, implemented by dividing the system into thin slabs parallel to the walls and rescaling the velocity regularly after every few iterations.

III. RESULTS

Our MD simulation shows that despite some similarities with amorphous solids at macroscopic scale [11–13], the flow behaviour of confined polycrystal is distinct. Although the externally applied body force (F_{ext}) is uniform, the interplay with the confining walls create spatially non-uniform stress. The polycrystalline solid yields due to this applied forcing, when the effective wall stress ($\sigma_w = \rho F_{ext}w/2$) exceeds a threshold which depends upon the channel width w [14]. Fig.1 shows an approximate state diagram, describing the state of the system (flowing or jammed) for a wide range of channel widths and driving forces. Further, we observe that while unjamming with the increase in F_{ext} , an intermediate state with stick-slip motion is observed (the shaded region in Fig.1); also see Fig-S1 in Supplementary Information (SI)[15]. Such states are also observed in yielding of amorphous systems [16] and even in channel flow of monodisperse colloids [17].

In the inset of Fig.1 we show average velocity profiles, for different channel widths (w), in steady state conditions. For large w , the flow profile of the soft polycrystal exhibits behaviour similar to yield stress fluids : $v_x(y)$ is plug-like at the central bulk region and has high, but nearly constant velocity gradient near the walls, resembling a boundary layer. In contrast, for narrow channels, the averaged flow profile $v_x(y)$ is parabolic, similar to low Reynolds number (viscous) pipe flow. This is consistent with the observations in dense, soft, glassy material [11] where such transition from plug to parabolic flow with decreasing channel width was rationalised via the existence of non-local spatial correlations in plasticity during flow. Beyond such similarities with amorphous solids in the average flow profiles, some distinct features arise in flowing polycrystals due to its underlying grain dynamics, and that is the focus of this work. In Fig.1, we show schematic pictures of the distinct grain morphologies (detailed later) that occur at different parts of the state diagram.

Now we discuss the typical steady state flow behaviour in the case of the wide channels, at low (Fig.2-a) and high (Fig.2-c) forces (see the state points marked in Fig.1). While fluid-like structure prevails in the boundary layer (more prominent in Fig.2-c than in Fig.2-a), polycrystalline grain structure is maintained in the bulk. The bulk, in both cases, exhibits plug-like flow profile, with the plug front moving at higher velocity at higher force. However, the grain structure, in both cases, constantly remodels via grain break-up and coalescence [10] (see movie in SI [15]). In Fig.2(a,c), we use the Ψ_6 hexatic order parameter (OP) representation to capture the local arrangement of the particles and also to clearly demarcate the grain boundaries.

This dynamic cycle of grain growth and breakage occurring in the bulk can be attributed to heterogeneity in the velocities of the particles across grains. The enclosed box in the bulk of Fig.2(a) is zoomed in subplot Fig.2(b) to illustrate this more clearly. It shows a moving triple junction of grains, where the grain boundaries are shown by broken lines. We see that particles constituting each grain have transverse motions in different directions within each grain. Similar velocity map for Fig.2(c), at higher force (and higher particle velocities), is shown and explained in the SI (Fig.S4) [15]. Further quantitative analysis in terms of non-homogeneous transverse velocities and strain rates, causing slow shear of the grains, are given by Fig.S2, Fig.S3 in SI [15]. We also illustrate that there are finite fluctuations in transverse velocity, $\langle \delta v_y^2(y) \rangle$, in the bulk, indicating existence of plastic events. Relatedly, there is indeed nonzero strain rate $\dot{\gamma} = \partial v_x / \partial y$ (shown in Fig-S3 of SI[15]), at the centre of the channel. However, the magnitude of the local shear-rate is much weaker at the middle compared to the boundary regime. This local shear leads to the continuous grain growth and break up near the centre. This heterogeneous dynamics can be quantified by studying the time evolution of the dislocation population N_d (Fig.S6, SI[15]), a marker that is distinct to polycrystals, compared to amorphous systems.

Distribution of particle displacements $P(u)$, where u is the magnitude of the 2D displacement, is an useful marker for spatio-temporal heterogeneity [3, 18]. In Fig.2(d) we show that $P(u)$, collected after different time intervals t (see Fig.S6, SI[15]), collapse onto a master curve, as should be the case for steady state conditions, when $P(u)$ and u are appropriately scaled. This implies a stationary pattern of displacements originating from different regions of the channel and the scaling can be understood from the average velocity profile. The dominant peak of $P(u)$ in Fig.2-b is populated by particles from the bulk region that exhibits plug flow. The nearly horizontal part of $P(u)$ comes from the boundary layers and can be rationalised as follows. The mean velocity profile $v(y) \approx \frac{y}{t}$ is approximately linear in y , the distance from the walls. In the distribution the particles with displacements between u and $u + du$ come from the strip of width dy and length L , thus $P(u)du \propto dy.L$. The linear profile near the wall gives $dy \propto du/t$. Using this

we get $P(u)t = \text{constant}$, i.e, $P(u)t$ is independent of u . Furthermore, to characterise the velocity fluctuation we define a non-dimensional velocity $\Delta v_x = \frac{v_x - \langle v_x(y) \rangle}{v_{rms}}$ where v_x is the instantaneous velocity along \hat{x} , $\langle v_x(y) \rangle$ is the average velocity and v_{rms} is the rms velocity. The non-dimensional velocity fluctuation shows a non-Gaussian distribution that deviates at the tails, see inset of Fig.2-b. Interestingly, similar non-Gaussian distribution has been reported in dense granular flows [19–21]. However, the distribution is highly asymmetric in case of dense granular flows which is notably different with polycrystal.

Qualitatively new flow behaviour emerges when the channel is narrow ($w \approx 10d$), and the rheological response is probed in the vicinity of the yield threshold ($\sigma_w = 6.4$); see the marked location in Fig.1. The moving polycrystal disintegrates into chunks of crystallites and fluid-like patches, along the length of the channel; see Fig.3. In the upper four panels (Fig.3(a)), we show time evolution of snapshots of particle positions, with time increasing upwards as indicated, using the Ψ_6 representation which clearly differentiates the crystalline and fluid zones. We also observe that the density in the fluid zone is relatively less. In Fig.3(b), we superpose the particle velocities, in few narrow vertical strips, corresponding to the panel just above it. It is evident that the particles in the fluid zones move fast while the crystalline zones are nearly static with small random velocities. Yet, the flow profile $v_x(y)$, averaged along the flow direction (\hat{x}), is parabolic (see inset of Fig.1), which is mainly contributed by the liquid like regions, where the profile is strongly parabolic. Thus, from the average flow profile, it is not possible to guess about the underlying density stratification. Although the solid-liquid interfaces are not sharp in Fig.3, it appears that the interface is moving left, in the opposite direction of the main flow. Before probing this in details, we note that density waves were reported in gravity-driven granular flows and traffic flows [22, 23]. Also, in experiments with driven, dense colloidal suspensions, backward moving density waves were reported [24, 25] and modelled [26]. However, note here, that in our case, we have no explicit solvent, as was invoked in discussing such observations in experiments [24] or for modeling [26].

To capture the motion of the diffuse liquid-solid interface, we constructed an effective coarse grained, 1-D density field by integrating the particle number density along \hat{y} . Fig.3(c) shows density snapshots at successive time intervals. The liquid patch (the low density dark region) can be seen moving to the left at nearly constant speed (as the kymograph is linear). To confirm this effect, in Fig3(d), we recorded the average particle velocity $\langle v_x(t) \rangle$ in a fixed area element, at the centre of the channel, as a function of time. Almost regular temporal oscillations can be seen. The corresponding Fourier transform of $|\langle \overline{v_x}(\omega) \rangle|$ shows a dominant peak and a weak first harmonic, see inset-2 in Fig3(d). In inset-1, we present the velocity distribution $P(v_x)$ of all the particles in the channel. The distribution is asymmetric and gets higher weightage from the positive side, implying that the average velocity is rightward, although there are local motions occurring in the opposite direction as well. We checked that the positive tail at high v_x is contributed by the fast moving liquid particles and the maxima at small positive v_x comes from the crystalline regions. The low density liquid patch moves backward essentially by treadmilling. Consider a liquid patch in between two solid blocks. The exposed layer from the left block melts into liquid due to F_{ext} and thermal forces, and the "atoms" move right due to F_{ext} . This way the left front of the liquid moves one atomic spacing to the left. At its right front, right moving "atoms" from the liquid, driven by F_{ext} add a new layer to the solid block on the right. So the right front of the liquid moves left by one unit. The melting occurs as F_{ext} overcomes cohesion force of the LJ solid and the melting rate is constant provided the number densities in both the solid and the liquid attain steady values at a particular temperature.

Note that in this mechanism a given particle periodically resides in the solid and liquid regions, and moves slow and fast accordingly. We rationalize the density wave generation along the same lines as in Ref[26], with one significant difference. The body force in our force balance equation (below) is dependent on particle number density, as in usual for gravity driven flows.

$$0 = \rho F_{ext} - \xi(\rho)v + \nu \frac{\partial^2 v}{\partial x^2}, \quad (1)$$

In this 1D equation, ρ is a spatially-varying number density, v is the velocity, F_{ext} is the applied external body force, ξ is the friction coefficient and ν is the effective viscosity. In SI-section-V [15], using linear stability analysis, we show that the density wave occurs only when the force F_{ext} is below some threshold value; we also verify this in our simulations. Such a threshold was absent in the findings of Ref[26].

Plug like flows have been well known in amorphous yield-stress materials [24, 27–29]. What is novel for flowing polycrystal is the coexistence of crystallinity and flow. Although velocity heterogeneity leads to remodelling of the grains, a polycrystalline morphology is still maintained during the plug flow. This is because grain remodelling rates are slow compared to the average velocity of the plug flow. Even flow transition from plug to parabolic profile at decreased channel width has been reported before for concentrated emulsions [11, 12, 30] and granular systems [31]. While these have been rationalised via non-local rheological models [30], in our system the transition is accompanied by clear morphological changes of the structure (schematic diagrams in Fig-1), and it occurs when the channel width is comparable to typical grain size, the relevant correlation length of our system. Thus, within the non-local rheological

models, these structural changes at the level of grains need to be incorporated as well.

IV. SUMMARY

In summary, we have illustrated how the interplay between grain size, the additional length scale in soft polycrystals, and the channel width result in contrasting Poiseuille flow for wide and narrow rough channels. At large channel width, the polycrystalline structure is retained in the visibly plug like region at the centre, although the continuous breakages and coalescences occur due to influence of the boundary. This, obviously, has no parallel in polydisperse emulsions or granular systems. However, for narrow channels, when the channel width becomes comparable to typical grain size, the polycrystalline structure significantly melts during flow and we observe a transverse density stratification, with a backward moving low density wave, analogous to flowing granular matter [32], colloids [24, 26, 33, 34] and even traffic flow in highways [23]. Interestingly, as the density stratification switches from parallel to transverse direction, at intermediate channel widths the boundary layer shows unstable, transverse incursions (Fig.S7, SI[15]), which stabilise as the width is further reduced. Our work should motivate further experimental exploration of such flow behaviour in colloidal polycrystals, in the context of increased interest in such materials.

-
- [1] S. Gokhale, K. H. Nagamanasa, R. Ganapathy, and A. Sood, *Soft Matter* **9**, 6634 (2013).
 - [2] H. Zhang and Y. Han, *Physical Review X* **8**, 041023 (2018).
 - [3] S. Biswas, M. Grant, I. Samajdar, A. Haldar, and A. Sain, *Scientific reports* **3** (2013).
 - [4] S. Gokhale, K. H. Nagamanasa, V. Santhosh, A. Sood, and R. Ganapathy, *Proceedings of the National Academy of Sciences* **109**, 20314 (2012).
 - [5] E. Tamborini, L. Cipelletti, and L. Ramos, *Physical review letters* **113**, 078301 (2014).
 - [6] I. Buttinoni, M. Steinacher, H. T. Spanke, J. Pokki, S. Bahmann, B. Nelson, G. Foffi, and L. Isa, *Physical Review E* **95**, 012610 (2017).
 - [7] F. A. Lavergne, A. Curran, D. G. A. L. Aarts, and R. P. A. Dullens, *Proceedings of the National Academy of Sciences* **115**, 6922 (2018).
 - [8] H. Shiba and A. Onuki, *Physical Review E* **81**, 051501 (2010).
 - [9] T. Hamanaka and A. Onuki, *Physical Review E* **74**, 011506 (2006).
 - [10] T. Sarkar, S. Biswas, P. Chaudhuri, and A. Sain, *Physical Review Materials* **1**, 070601 (2017).
 - [11] J. Goyon, A. Colin, G. Ovarlez, A. Ajdari, and L. Bocquet, *Nature* **454**, 84 (2008).
 - [12] V. Mansard, A. Colin, P. Chaudhuri, and L. Bocquet, *Soft matter* **9**, 7489 (2013).
 - [13] P. Chaudhuri and J. Horbach, *Physical Review E* **90**, 040301 (2014).
 - [14] P. Chaudhuri, V. Mansard, A. Colin, and L. Bocquet, *Physical review letters* **109**, 036001 (2012).
 - [15] Supplementary Material (with more analysis), which includes Refs. ([26, 35, 36]).
 - [16] F. Varnik and D. Raabe, *Physical Review E* **77**, 011504 (2008).
 - [17] D. Genovese and J. Sprakel, *Soft Matter* **7**, 3889 (2011).
 - [18] P. K. Jana, M. J. Alava, and S. Zapperi, *Scientific Reports* **7**, 45550 (2017).
 - [19] S. Moka and P. R. Nott, *Physical review letters* **95**, 068003 (2005).
 - [20] A. V. Orpe and A. Kudrolli, *Physical review letters* **98**, 238001 (2007).
 - [21] K. Ananda, S. Moka, and P. R. Nott, *Journal of Fluid Mechanics* **610**, 69 (2008).
 - [22] E. D. Liss, S. L. Conway, and B. J. Glasser, *Physics of Fluids* **14**, 3309 (2002).
 - [23] B. S. Kerner and P. Konh user, *Physical Review E* **48**, R2335 (1993).
 - [24] L. Isa, R. Besseling, A. N. Morozov, and W. C. K. Poon, *Phys. Rev. Lett.* **102**, 058302 (2009).
 - [25] S. Horikawa, A. Nakahara, T. Nakayama, and M. Matsushita, *Journal of the Physical Society of Japan* **64**, 1870 (1995).
 - [26] P. Kanehl and H. Stark, *Phys. Rev. Lett.* **119**, 018002 (2017).
 - [27] M. T. Roberts, A. Mohraz, K. T. Christensen, and J. A. Lewis, *Langmuir* **23**, 8726 (2007).
 - [28] J. C. Conrad and J. A. Lewis, *Langmuir* **24**, 7628 (2008).
 - [29] A. Nikoubashman, G. Kahl, and C. N. Likos, *Soft Matter* **8**, 4121 (2012).
 - [30] L. Bocquet, A. Colin, and A. Ajdari, *Physical review letters* **103**, 036001 (2009).
 - [31] K. Kamrin and G. Koval, *Physical Review Letters* **108**, 178301 (2012).
 - [32] S. Horikawa, T. Isoda, T. Nakayama, A. Nakahara, and M. Matsushita, *Physica A: Statistical Mechanics and its Applications* **233**, 699 (1996).
 - [33] M. Haw, *Physical review letters* **92**, 185506 (2004).
 - [34] A. I. Campbell and M. D. Haw, *Soft Matter* **6**, 4688 (2010).
 - [35] E. G. Daub and J. M. Carlson, *Physical Review E* **80**, 066113 (2009).
 - [36] J. M. Tarp, L. Angheluta, J. Mathiesen, and N. Goldenfeld, *Physical review letters* **113**, 265503 (2014).

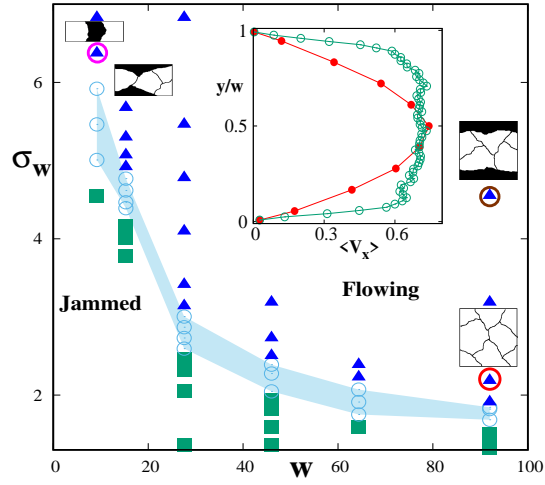


FIG. 1. Phase plot as a function of channel width w and wall stress σ_w . Three different dynamical states are identified: flowing (triangles), stick-slip (circles) and jammed (squares). The shaded region represents the stick-slip states. In the flowing state stratification of the system into polycrystalline and liquid like zones (shaded) are indicated by schematic diagrams. The inset shows the averaged velocity profile $v_x(y)$ plotted as a function of y/w . The flow exhibits plug and parabolic profiles, for wide (open circles) and narrow (solid circles) channels, respectively. The corresponding parameters are $(w, \sigma_w) = (9.2, 6.4)$ and $(92, 2.2)$.

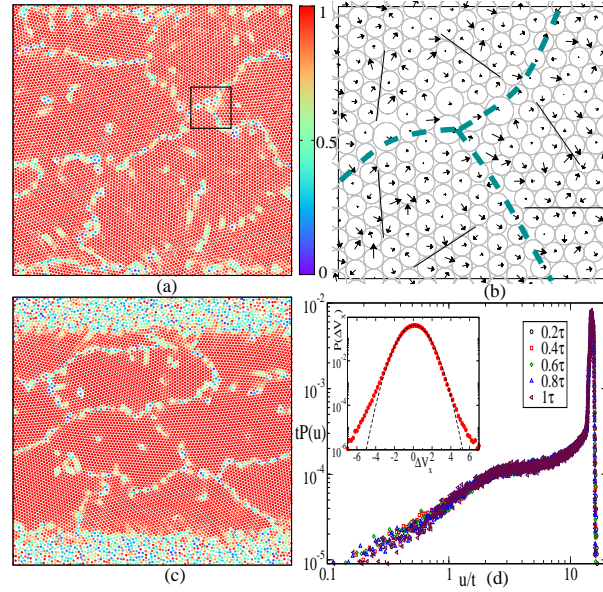


FIG. 2. Flowing grains in a wide channel ($w = 92$), at low (a) and high (c) driving forces, $\sigma_w = 2.2$ and 4.6 , respectively. Colour bar shows hexatic order parameter, Ψ_6 , value. A significant boundary layer (BL) emerges at high force. A triple grain junction in (a) is zoomed in subplot (b), and velocity vectors added, in order to show the velocity heterogeneity among grains. (d) Scaled displacement distributions for different time intervals t (symbols shown in legend-box) collapse. The inset shows distribution of nongaussian velocity fluctuation (for case-c) along the flow.

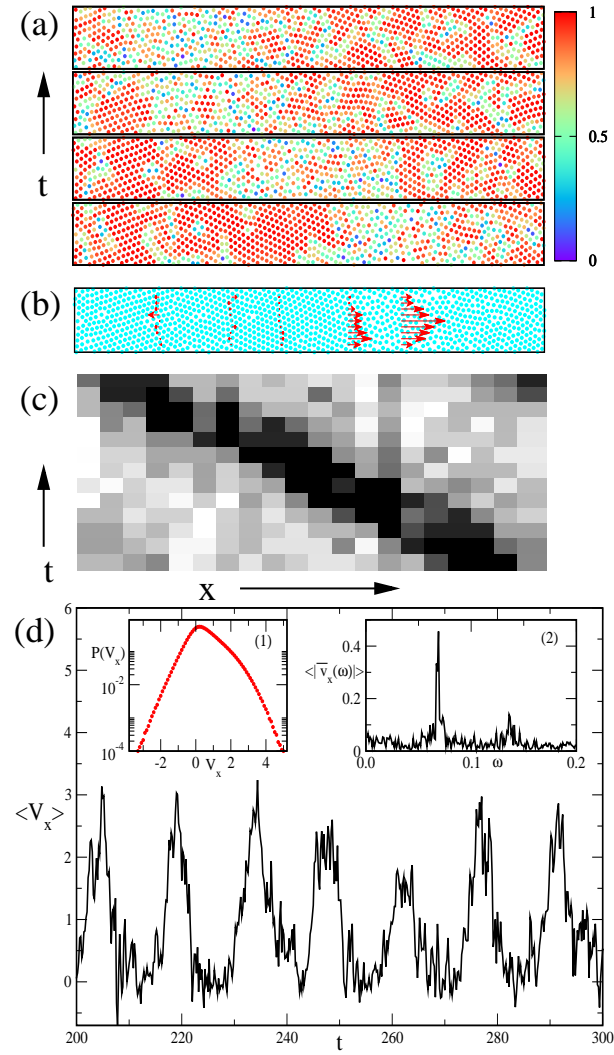


FIG. 3. Fluidization of a flowing polycrystal in narrow channel ($w = 9.2, \sigma_w = 6.4$). (a) The four panels show a moving patch of fluid, with time increasing upwards. Colour bar shows value of Ψ_6 OP. (b) Shows heterogeneous velocity map in the earliest snapshot, on five vertical strips. In the corresponding density map (c), the fluid front moves left, opposite to the main flow; darker the colour, lower the density. (d) Average particle velocity $\langle v_x \rangle$ in an area element at the channel centre. Nearly periodic oscillations imply that the liquid patch moves at a constant speed across the channel. Inset-1 shows skewed velocity distribution $P(v_x)$ of all particles. The peak in inset-2 confirms the periodicity in $\langle v_x \rangle$.